Construction of 3D Metallic Nanostructures on an Arbitrarily Shaped Substrate

Fei Chen, Jingning Li, Fangfang Yu, Di Zhao, Fan Wang, Yanbin Chen, Ru-Wen Peng, and Mu Wang**

Future information technology relies on our capability to fabricate microstructures with functional materials. Current microfabrication technology transfers geometrical patterns to a material surface coated with chemical photoresist by using mask (photolithography) or via scanning electron beam (electron beam lithography).[1,2] Subsequently, a series of chemical treatments are applied either to engrave the exposure pattern on the material surface underneath the photoresist, or to hollow out a desired pattern on the photoresist and enable deposition of a new material upon the substrate.[3,4] Yet conventional lithography process requires a flat substrate in order to guarantee homogeneous pattern transfer. If the substrate surface is irregularly bumpy, photolithography-based technique becomes less efficient: for the etching process, material in the concave region is difficult to be removed than those in the convex region; for the deposition process, per contra, those in the convex region deposits faster than that in the concave region. Such effect is an intrinsic nature of concentration field in etching/growth process and cannot be easily resolved.[5–7]

On the other hand, in order to shorten information access time and to increase the degree of integration, there is an increasing demand to develop 3D fabrication methods for microelectronics and spintronics.[8–11] For example, racetrack memory has been proposed as a nonvolatile memory device based on the controlled motion of magnetic domain walls in nanowires driven by pulses of spin-polarized electric current, where the nanowires are configured as standing U-shapes on the substrate.[8,12] Yet it is challenging to fabricate such structures with traditional fabrication approaches.

Self-organized growth has been proven to be efficient, especially in fabricating nanowires.[13,14] However, it remains challenging to generate spatially ordered metallic nanowire arrays with easy-controlled wire width and interwire separation. For example, closely packed nanopores in anodic alumina can be applied as template to grow nanowires, where diameter of the grown nanowires is determined by the size of nanopores, and cannot be freely tuned.[14–16] The other limitation of this approach is that the long-range order among the nanowires cannot be maintained once the alumina template is removed. So some other methods have to be developed to align the nanowires.[17–19] By introducing monolayer stripes on substrate and taking the advantage of selective nucleation on the patterned region, metallic nanowire array can indeed be made two-dimensionally.[6,7,20] Yet in this case, the spatial periodicity and line width of the wires remain untunable.

Here we report an unprecedented fabrication approach that allows to construct metallic (cobalt) nanowires on an arbitrarily shaped surface. The spatial separation of adjacent cobalt nanowires can be selected from 70 to 3000 nm and the line width varies from 50 to 250 nm by tuning the applied voltage in electrodeposition. Essentially this fabrication approach is based on an ultrathin film growth technology with controlled periodic fluctuation of film thickness, followed by ion beam etching to remove the webbed film connecting the neighboring ridges. Hence the growth direction of the nanowire is perpendicular to its longitudinal axis, which is contrary to the conventional sense of nanowire growth, and a desired 3D configuration of nanowires can be realized with a predesigned shaped substrate. Our discovery reveals the possibility to construct 3D nanowire arrays on an arbitrarily shaped surface with wet electrochemistry, and is inspiring in fabricating magnetic nanostructures for spintronic studies.

The cobalt wire arrays are electrodeposited from an ultrathin aqueous electrolyte solution of $CoSO_4$. The electrolyte (with initial concentration 0.02 M) and two straight, parallel cobalt electrodes are sandwiched by a glass plate and the substrate plate. The substrate can be either a polished silicon surface, or a grating with periodic ridge lines, or even a bumpy, unpolished silicon surface. Unlike conventional electrodeposition process, here we freeze the sandwiched electrolyte layer by a Peltier element underneath the growth cell.[6,7,21–26] During the solidification, $CoSO_4$ is partially expelled from the ice of electrolyte due to the partitioning effect.[24] When equilibrium is reached, an ultrathin layer of concentrated $CoSO_4$ electrolyte is formed between the ice of electrolyte and the substrate. At −4 °C the thickness of this ultrathin layer is of the order of 200 nm.[21] Instead of applying a potentiostatic signal across the electrodes,[6,7,21–26] here we apply a sine-shaped signal superposed on a constant voltage.

In potentiostatic electrodeposition of copper, it has been observed that at low applied constant voltage (1.5 V), the electrodeposit may form a compact thin film transversally developing on the substrate (**Figure 1**a(i)).[25] We also observed that in electrodeposition the interfacial growth may spontaneously turn oscillatory,[21–25] generating periodic growth striations on the metallic deposit. The unique feature of this growth system is that the nucleation barrier for metallic crystallite at the concave corner of the substrate and the metal deposit (site 1 in

Dr. F. Chen, J. Li, F. Yu, D. Zhao, F. Wang,
Prof. Y. Chen, Prof. R.-W. Peng, Prof. M. Wang
National Laboratory of Solid State Microstructures
and School of Physics, and Collaborative Innovation
Center of Advanced Microstructures
Nanjing University
Nanjing 210093, P. R. China
E-mail: rwpeng@nju.edu.cn; muwang@nju.edu.cn

DOI: 10.1002/adma.201602049

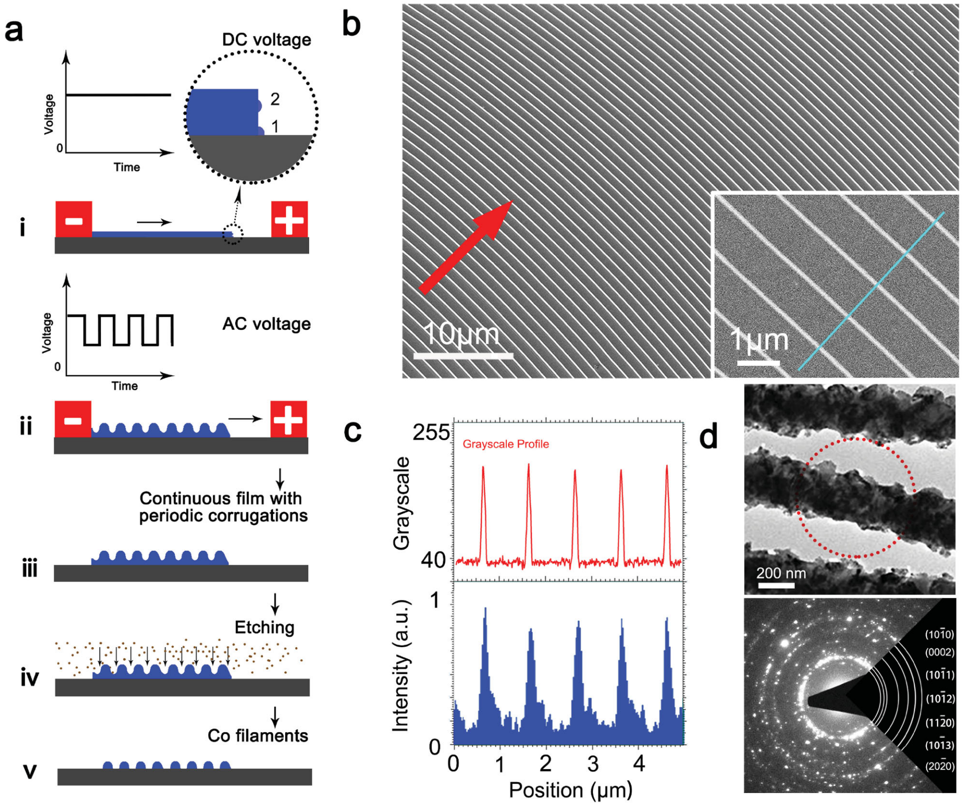

Figure 1. The schematic illustration of the fabrication process, nanowire morphology, chemical element distribution across the nanowire array, and the electron diffraction pattern of the nanowires. a) The schematics of the fabrication process of the nanowire array. b) SEM micrograph of the cobalt nanowire array generated by applying a voltage with static component 1.5 V plus a sine-shaped oscillatory component with amplitude 0.55 V and frequency 1 Hz. The red arrow denotes the growth direction of the wire array. The inset shows the details of the nanowire array, where the green line indicates the scanning line for EDS analysis. c) The topography and chemical element analysis of the nanowire array. The red curve represents the grayscale profile along the green line marked in (b); the blue line represents cobalt element distribution along the green line in (b), which is obtained by EDS analysis. d) The bright-field TEM image of the nanowire and electron diffraction pattern of the selected area. The diffraction pattern indicates that the nanowire is polycrystalline and possesses hcp structure. Seven diffraction rings are identified from the inner part of the diffraction pattern to the outside, the corresponding indexes are listed from top to bottom on the right side of the diffraction pattern.

Figure 1a(i)) is always lower than the other places (site 2, for example).[27] Consequently, a compact metal film can grow firmly on the substrate.[7] With a higher applied voltage across the electrodes, the nucleation rate of metallic crystallites becomes higher. Consequently, the film thickness becomes higher. In present experiment, the designed periodic voltage across the electrodes contributes to the formation of nanoridges with well-defined spatial periodicity on an ultrathin metallic film (Figure 1a(ii)). Thereafter, by Ar^+ beam etching the webbed film between the ridges can be removed (Figures 1a(iv,v)). In this way, an array of metallic nanowires with specific spatial separation is fabricated (Figure 1a(v)). We need to point out that conventionally a nanowire develops in the direction along the wire axis, which is often promoted by the catalyst sitting on the tips of the wires. In our case, formation of the nanowire occurs simultaneously over the whole wire, with both line-width and wire-separation independently controllable by the applied voltage.

Figure 1b shows a typical morphology of cobalt filament array formed on the surface of a flat silicon substrate, where the red arrow denotes the growth direction of the electrodeposit, which is perpendicular to the long axis of the wire. The area of uniform nanowire arrays can easily reach over 100 µm × 100 µm. The inset of Figure 1b illustrates the details of nanowire arrays. The green line marks the trajectory where energy-dispersive X-ray spectroscopy (EDS) has been analyzed. Figure 1c shows the profile of topography of nanowire array and the cobalt element distribution based on EDS analysis along the green line shown in Figure 1b. The step size for line scan of EDS analysis is 20 nm. Figure 1b,c provides an unambiguous evidence that the array of cobalt nanowires has been fabricated in a unconventional way.

Transmission electron microscopy (TEM) is applied to characterize the microstructure of the metallic nanowire. Figure 1d shows the bright field image (top) and electron diffraction pattern (bottom) of the selected area on the nanowire. The sample of the nanowires is obtained by etching the electrodeposit on a copper TEM grid. The electron diffraction indicates that the nanowires are polycrystalline and possess hcp structure.

The spatial periodicity of nanowires is controlled by tuning the frequency of applied oscillating signal (**Figure 2**a–d). By changing the frequency from 0.5 to 8 Hz and maintaining the rest of parameters (amplitude of oscillating signal 0.55 V, potentiostatic voltage 1.5 V, initial concentration 0.02 M,

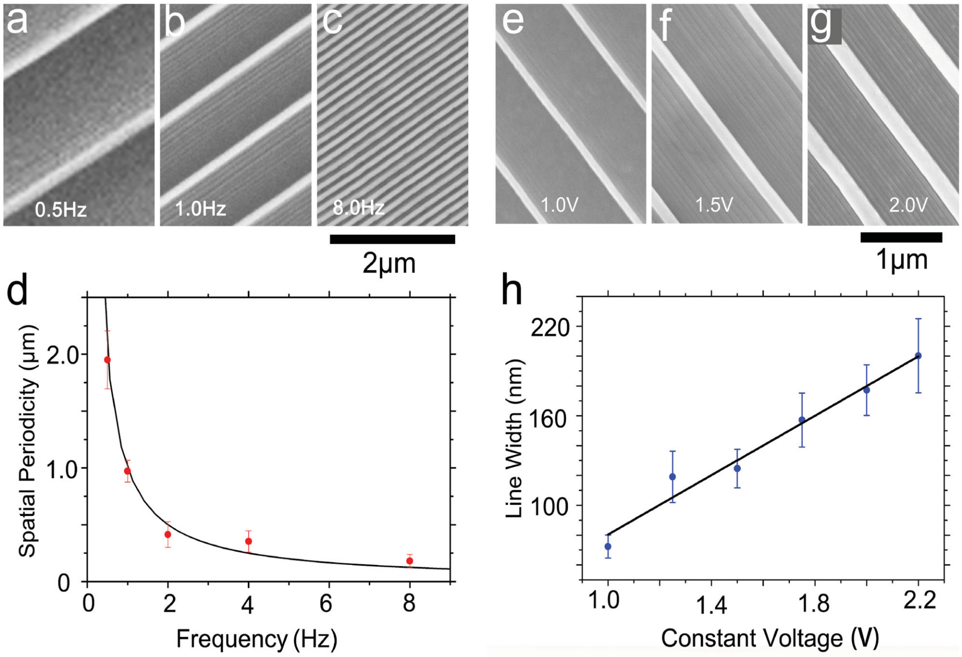

Figure 2. Dependence of spatial periodicity and line width of the nanowire array and control parameters in electrodeposition. a–d) The dependence of the spatial periodicity of cobalt wire array and the frequency of applied oscillating voltage across the electrodes. (a–c) show SEM micrographs of cobalt nanowire arrays grown at the corresponding frequency of the applied voltage, respectively. e–h) The dependence of line width of the cobalt wire and the static component of the applied voltage across the electrodes. e–g) SEM micrographs of cobalt nanowire array with different line width.

temperature –4 °C), the spatial separation of the nanowires decreases from 1800 to 150 nm accordingly. A series of experiments have been carried out and we conclude that the spatial periodicity is inversely proportional to the frequency, as shown in Figure 2d. From the inset of Figure 2b, one may identify some wrinkles in between the wires, which represents oscillation of thickness of webbed film and is induced by spontaneous concentration oscillation of electrolyte in electrodeposition.[13,22] The thickness of the webbed film is of the order of 40 nm. This film can be removed by gentle Ar^+ beam etching. The minimum spatial separation of the adjacent wires achieved so far is 70 nm.

The width of the nanowire is controlled by the potentiostatic component of the applied voltage across the electrodes. Experimentally we find that by tuning the constant voltage across the electrodes from 1.1 to 2.2 V, and keeping rest of parameters constant (oscillating signal frequency 1.0 Hz, amplitude 0.55 V, initial concentration 0.02 M, temperature –4 °C), the width of nanowire increases accordingly from 92 to 235 nm, as illustrated in Figure 2e–h.

Most interestingly, this electrodeposition process can be applied on a substrate with arbitrary surface landscape. To demonstrate this capability, we select a polymer grating surface with closely packed ridges (spatial separation 1400 nm, height 200 nm) as substrate for electrodeposition. The cobalt nanowires climb up and down following the topography of substrate, and both spatial periodicity and line width of the nanowires are homogeneous across the grating surface, as illustrated in **Figure 3**a,b. Further, we carry out electrodeposition on an unpolished single-crystalline

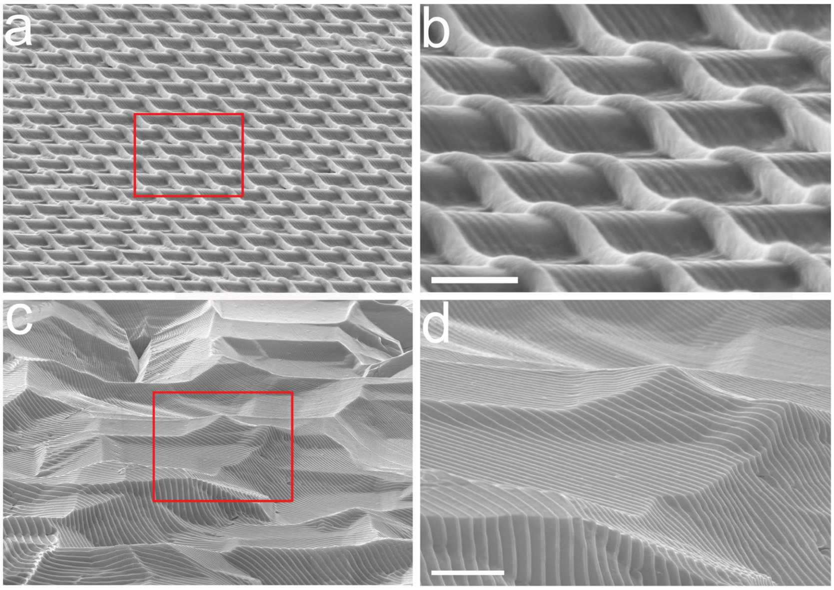

Figure 3. Growth of nanowire array on the arbitrarily shaped substrates. a,b) The micrographs of nanowire arrays grown on a grating surface are shown. One may find that the cobalt wire just follows the variation of substrate topography and forms a 3D wavy structure. c,d) Cobalt nanowire array grown on an unpolished single-crystalline silicon surface. The bars in (b) and (d) represent 500 nm and 2 μm, respectively.

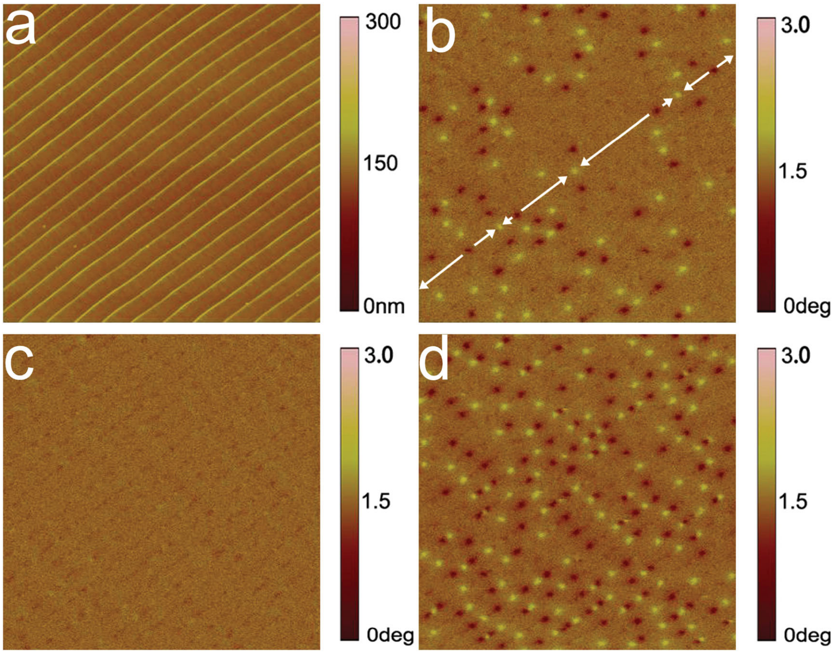

Figure 4. MFM micrographs of cobalt nanowire array on a flat substrate. a) Topographic micrograph of the nanowire arrays (after Ar$^+$ beam etching). b) The corresponding initial magnetic domain structures of the nanowire arrays. The white arrows denote the directions of spin polarization. The dark point corresponds to a tail-to-tail domain wall and the bright point corresponds to head-to-head domain wall. c) The remanence magnetic state after a magnetic field of 0.6 T is applied in-plane along the direction of the nanowires. d) The remanence magnetic state after a magnetic field of 0.6 T is applied perpendicular to the substrate surface and the nanowires. The scan size of these micrographs is 30 μm × 30 μm.

silicon surface as shown in Figure 3c,d, where micrometer-scale height fluctuation can be found everywhere and many facets and edges form either obtuse or sharp angles. Figure 3c,d demonstrates the cobalt nanowire array grown on this bumpy surface with aforementioned method, and the width and the separation between nanowires maintain constant. As illustrated in Figure 3c,d, at some locations the edge of neighboring facets is really sharp, yet metallic wires develop on the bumpy surface following the local surface topography and the contour of concentration field and electric field.

Magnetic force microscopy (MFM) has been employed to characterize the magnetic structures of the cobalt nanowires. Micrograph of an Ar$^+$-etched cobalt nanowire array grown on a flat silicon substrate is illustrated in **Figure 4**a. The corresponding MFM micrograph is illustrated in Figure 4b, where the site corresponding to the head-to-head magnetic domain walls is illustrated as bright (dark) spot, and the site corresponding to the tail-to-tail domain walls is illustrated as dark (bright) spot. In Figure 4b, the white arrows denote the directions of local spin polarization. The magnetic state in nanowires upon applying an external magnetic field in different directions has also been investigated. When a magnetic field of 0.6 T is applied in the direction along nanowires and is gradually reduced to zero, the magnetic polarization of nanowire aligns with the long axis of the wire. Meanwhile, almost no stray field can be detected, as demonstrated in Figure 4c. When a magnetic field of 0.6 T is applied perpendicular to the substrate (and hence perpendicular to nanowires) and is subsequently reduced to zero, head-to-head and tail-to-tail magnetic domain walls reemerge with a larger domain-wall density, as shown in Figure 4d. In this case, substrate surface is flat and the domain walls are randomly distributed.

The spin polarization in nanowires can be understood as follows. The easy axis of magnetization of a nanowire is along the longitudinal axis of the wire. When an external magnetic field is applied along nanowire, magnetization becomes uniform along the nanowires. This is a state with lowest total magnetic energy. Therefore, once external magnetic field is removed, the magnetic state resumes. If the applied magnetic field becomes perpendicular to the nanowires, the magnetization is uniformly perpendicular to the nanowires. Yet this scenario corresponds to a state with higher magnetic energy. Consequently, once the applied magnetic field is removed, magnetic moment will rotate to the direction either parallel or antiparallel to the nanowire. In this way, a number of head-to-head and tail-to-tail domain walls emerge randomly in the wire.

Nowadays conventional planar devices in spintronics are approaching the scaling limit, so it is necessary to explore more cost-effective ways to fabricate 3D magnetic structures for data storage. Self-organized route is promising to minimize the production costs. To test the feasibility, we fabricate 3D magnetic nanowire arrays on patterned substrates. **Figure 5**a shows the morphology of nanowire arrays grown on a polymer grating surface, where the wide stripes pointing from lower right to upper left are the gratings, and the narrow wires in the direction from lower left to upper right are the cobalt nanowires (the webbed film connecting adjacent nanowires has been etched off). The initial magnetic state of the cobalt wire array is illustrated in Figure 5b, where a number of pairs of bright–dark spots can be identified, which designate the stray field of the magnetic structures in the wires. It is interesting to note that in between the pairs of bright–dark spots with high contrast, there are a number of faint bright–dark spot pairs. To understand the spin polarization along nanowires, we apply a magnetic field parallel to the nanowires and study the remanence magnetic state, as illustrated in Figure 5c. It turns out that along the nanowire there are a series of faint bright–dark spot pairs, which designate the weak stray field induced by the geometrical bending of nanowires when they climb across the grating ridges. Figure 5e shows the enlarged MFM micrograph with superposed topography. One may identify that when the nanowire climbs up and steps down the grating ridge, two pairs of faint bright–dark spots are generated. It should be noted that here the detected weak stray field is associated with geometrical bending of wires, which is much weak comparing to that induced by the domain walls.

Figure 5d illustrates the remanence magnetic state of nanowires after applying a magnetic field perpendicular to

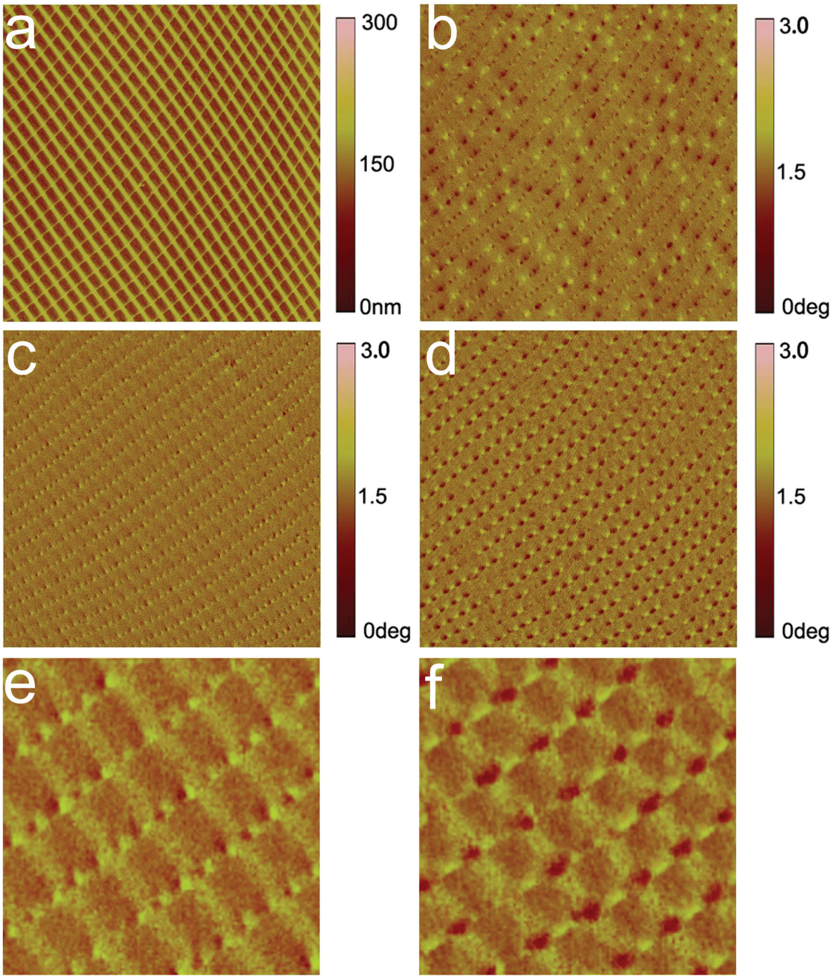

Figure 5. MFM micrographs of nanowire arrays grown on a grating surface. a) The topographic micrograph of the nanowire array grown on a grating surface after ion-beam etching. b) The corresponding initial magnetic domain structures of the nanowire array. Two types of spot-pairs can be identified: one is large bright–dark spot pair with higher contrast; the other is tiny bright–dark spot-pair with faint contrast. In the initial state the appearance of these two magnetic structures is random in position. c) The remanence magnetic state after applying a magnetic field of 0.6 T in the plane of substrate along the direction of nanowires. A series of faint bright–dark spot pairs can be observed along the wires. d) The remanence magnetic state after applying a magnetic field of 0.6 T perpendicular to the substrate. A series of bright–dark spot pairs with much higher contrast can be observed. The scan size for (a–d) is 30 μm × 30 μm. e) The enlarged MFM of (c) superposed with topography information. One may find that when the nanowire climbing up and stepping down the grating ridge, both generate a pair of bright–dark spots, with faint contrast. We expect that in this scenario the spin polarization is along the nanowire, and the stray field detected by MFM is due to the bending of the wire when it climbs across the ridge of the grating. f) The enlarged MFM of (d) superposed with topography information. One may find that the dark spots correspond to the top of the ridge of the grating, and bright spots correspond to the sites in between two grating ridges. The scan size for (e,f) is 7.5 μm × 7.5 μm.

the substrate. In this case, an array of bright–dark spots with high contrast emerges. Figure 5f illustrates the enlarged MFM micrograph with superposed topography. It can be identified that when the nanowire is on the top of a grating ridge, a dark spot appears on MFM. A bright spot appears in the valley between the neighboring grating ridges. This MFM suggests that domain walls are orderly distributed following the spatial periodicity of grating. Comparing Figure 5c–f, one may understand the physics of the MFM pattern in Figure 5b: the initial magnetic state of nanowires on the grating surface is a mixture of the polarization along the wire with some domain walls. The bright–dark spot pairs with higher contrast are contributed by the domain walls, while those faint bright–dark spot pairs, usually appear in two pairs at least, are induced by the stray field when a nanowire climbs across the grating ridges.

The electrochemical growth shown here demonstrates a unique transversal fabrication approach of nanowire arrays. As we stated earlier, spatial separation of nanowires depends on the frequency of applied oscillating signal when electrolyte concentration, potentiostatic voltage across the electrodes, and temperature for electrodeposition remain constant. Yet if the frequency of oscillating signal is higher than 10 Hz, the response of the system will not catch up with the driving frequency. This restricts the smallest spatial periodicity of the wire arrays to ≈70 nm. Similarly, the amplitude of the oscillating signal should be large enough to decouple the spontaneous oscillation.[23] However, if the applied voltage is over 2.5 V, system will risk instability. Therefore, in our system the largest nanowire width is about 220 nm. The other limitation of this fabrication approach is that the substrate should be nonconductive. Only in this way, lateral growth along the substrate surface from the cathode to anode can be guaranteed.

To date there are many ways to fabricate nanowires with certain diameter and chemical composition. However, it remains challenging to fabricate robust, spatially ordered 3D metallic nanowire arrays. For example, nanopores in anodic alumina has been applied to fabricate ordered nanowire array.[14–16] Yet the limitation of this approach is that the diameter of nanowires is determined by the size of nanopores. Besides, the long-range ordering among the nanowires disappears when the alumina template is removed.[15] Taking the advantage of favorable thermodynamic nucleation condition at the concave corner along the edge of a polymer stripe and the silicon substrate, we once revealed that the metallic wires prefer to nucleate and develop along the stripe, and the width of the metallic wires depends on the applied voltage in electrodeposition.[6,7] However, even so, the separation between neighboring nanowires remains determined by the selected template.[6,7] The fabrication method reported in this letter, however, represents a significant development in fabricating metallic nanowires: both the width and the separation of the nanowires can be independently tuned by externally applied electric voltage for electrodeposition, and the array can be fabricated on a substrate with arbitrary surface topography.

This fabrication approach is not limited to cobalt nanowires only. Instead, it can be applied to fabricate any metal/alloy material that can be electrochemically deposited. In fact, we have successfully deposited nanowires of copper, nickel–iron alloy, and cobalt–nickel alloy with this approach.[28] The capability to construct either conducting wire array or soft magnetic wire array on a surface with any topography will facilitate new approaches to manufacture stereo nanowire-based devices, such as domain-wall racetrack memory, nanowire transistors, flash memory, and gas sensors.[29–31] Our discovery may have impact on spintronics/microelectronics studies and will inspire further investigation in designing 3D devices.

Experimental Section

In order to generate the ultrathin electrolyte layer for electrodeposition, a thermostat circulator (Cole Parmer, Polystat 12108-35) and a Peltier element were used to decrease the temperature of the electrodeposition cell and to solidify the electrolyte. Detailed description of the electrodeposition system could also be found in references.[6,7,13,21–26] The cell for electrodeposition consisted of two parallel, straight electrodes made of cobalt wires 0.1 mm in diameter (Alfa Aesar, 99.995%). The horizontal separation of the electrodes was fixed as 6 mm. The electrodes were bounded by two rigid boundaries made of a microscope cover glass and a silicon wafer (or a grating/unpolished single-crystalline wafer). The electrolyte solution was prepared by dissolving analytical regent $CoSO_4$ (Alfa Aesar, 99.5%) in deionized water (Millipore, electric resistivity 18.2 MΩ cm). The initial concentration of $CoSO_4$ aqueous electrolyte was 0.02 M. The temperature of electrodeposition cell was carefully decreased to −4 °C. During solidification of electrolyte, $CoSO_4$ was partially expelled from the ice of electrolyte due to the partitioning effect,[24] which increased the local concentration of $CoSO_4$ in front of the solid–liquid interface. Consequently, local solidification point of electrolyte was further decreased (due to the concentrated electrolyte solution). This process continued until equilibrium was reached. Meanwhile, an ultrathin, concentrated unfrozen layer of aqueous electrolyte of $CoSO_4$ was trapped between the ice of electrolyte and the substrate. It was within this ultrathin electrolyte layer that the electrodeposition was carried out. Great care should be taken in the solidification process and several nucleation-melting cycles were repeated, so eventually there was only one ice nucleus in the electrolyte layer.[21–26] The temperature decrease rate was kept as low as about 0.1 °C h^{-1} in order to keep a flat solid–liquid interface. The ice of electrolyte kept growing, and reached the edge of the cell. The thickness of the ice increased continuously until equilibrium was reached. The thickness of the ultrathin layer of electrolyte trapped between the ice and the flat substrate depended on temperature, initial concentration of electrolyte, and amount of electrolyte solution in the deposition cell.[22] In this system, the thickness of this layer was of the order of a few hundreds of nanometers.[6,22] By applying certain voltage across the electrodes, cobalt filaments initiated from the cathode, deposited on substrate surface, and moved toward the anode.

In these experiments, a constant voltage superposed with a sine-shaped oscillatory voltage across electrodes was applied by a signal generator (SONY, AFG320). The constant voltage, frequency, and amplitude of the sine signal could be freely tuned. After electrodeposition, the cobalt electrodeposits was rinsed with ultrapure water and dried in a vacuum chamber for further analysis. The morphology of cobalt nanowires was characterized by a field-emission scanning electron microscope (SEM, Zeiss, ULTRA 55) and a multimode atomic force microscopy (Digital Instruments, Nanoscope IIIa). To remove the webbed film between the nanowires, ion beam etching was carried out with Ar^+ milling system (VN IBE150) and the etching rate of cobalt element was calibrated in advance.

The magnetic structures in the cobalt nanowires were characterized by MFM. The element distribution was characterized by energy dispersive X-ray analysis (EDAX, Oxford Instrument) at 10 keV. The nanowire arrays were magnetized by homemade Helmholtz coils, which generated a maximum magnetic field of 0.6 Tesla.

Acknowledgements

This work has been supported by grants from the State Key Program for Basic Research from MOST of China (Grant No. 2010CB630705 and 2012CB921502), and NSF of China (Grant Nos. 11474157 and 61475070).

Received: April 18, 2016
Revised: May 20, 2016
Published online: June 13, 2016

---

[1] C. Wagner, N. Harned, *Nat. Photonics* **2010**, *4*, 24.
[2] S. Kim, B. Marelli, M. A. Brenckle, A. N. Mitropoulos, E. S. Gil, K. Tsioris, H. Tao, D. L. Kaplan, F. G. Omenetto, *Nat. Nanotechnol.* **2014**, *9*, 306.
[3] D. Qin, Y. Xia, G. M. Whitesides, *Nat. Protoc.* **2010**, *5*, 491.
[4] W. Chao, B. D. Harteneck, J. A. Liddle, E. H. Anderson, D. T. Attwood, *Nature* **2005**, *435*, 1210.
[5] A. S. Filatov, M. V. Ferguson, S. N. Spisak, B. Li, C. F. Campana, M. A. Petrukhina, *Cryst. Growth Des.* **2013**, *14*, 756.
[6] B. Zhang, Y. Y. Weng, X. P. Huang, M. Wang, R. W. Peng, N. B. Ming, B. Yang, N. Lu, L. Chi, *Adv. Mater.* **2009**, *21*, 3576.
[7] M. Zhang, S. Lenhert, M. Wang, L. Chi, N. Lu, H. Fuchs, N. B. Ming, *Adv. Mater.* **2004**, *16*, 409.
[8] S. Parkin, S. Yang, *Nat. Nanotechnol.* **2015**, *10*, 195.
[9] J. R. Tumbleston, D. Shirvanyants, N. Ermoshkin, R. Janusziewicz, A. R. Johnson, D. Kelly, K. Chen, R. Pinschmidt, J. P. Rolland, A. Ermoshkin, E. T. Samulski, *Science* **2015**, *347*, 1349.
[10] R. Galland, P. Leduc, C. Guérin, D. Peyrade, L. Blanchoin, M. Théry, *Nat. Mater.* **2013**, *12*, 416.
[11] Y. Hayamizu, T. Yamada, K. Mizuno, R. C. Davis, D. N. Futaba, M. Yumura, K. Hata, *Nat. Nanotechnol.* **2008**, *3*, 289.
[12] S. Parkin, M. Hayashi, L. Thomas, *Science* **2008**, *320*, 190.
[13] M. Wang, S. Zhong, X. B. Yin, J. M. Zhu, R. W. Peng, Y. Wang, K. Q. Zhang, N. B. Ming, *Phys. Rev. Lett.* **2001**, *86*, 3827.
[14] H. Masuda, K. Fukuda, *Science* **1995**, *268*, 1466.
[15] W. Lee, H. Han, A. Lotnyk, M. A. Schubert, S. Senz, M. Alexe, D. Hesse, S. Baik, U. Gösele, *Nat. Nanotechnol.* **2008**, *3*, 402.
[16] P. Banerjee, I. Perez, L. Henn-Lecordier, S. Lee, G. Rubloff, *Nat. Nanotechnol.* **2009**, *4*, 292.
[17] R. Laocharoensuk, K. Palaniappan, N. A. Smith, R. M. Dickerson, D. J. Werder, J. K. Baldwin, J. A. Hollingsworth, *Nat. Nanotechnol.* **2013**, *8*, 660.
[18] J. Yao, H. Yan, C. M. Lieber, *Nat. Nanotechnol.* **2013**, *8*, 329.
[19] N. O. Weiss, X. F. Duan, *Nat. Nanotechnol.* **2013**, *8*, 312.
[20] W. C. Lee, K. Kim, J. Park, J. Koo, H. Y. Jeong, H. Lee, D. A. Weitz, A. Zettl, S. Takeuchi, *Nat. Nanotechnol.* **2015**, *10*, 423.
[21] X. P. Huang, Z. L. Shi, M. Wang, M. Konoto, H. S. Zhou, G. B. Ma, D. Wu, R. W. Peng, N. B. Ming, *Adv. Mater.* **2010**, *22*, 2711.
[22] Y. Y. Weng, J. W. Si, W. T. Gao, Z. Wu, M. Wang, R. W. Peng, N. B. Ming, *Phys. Rev. E* **2006**, *73*, 051601.
[23] F. Chen, F. Wang, F. Jia, J. N. Li, K. Liu, S. X. Huang, Z. Z. Luan, D. Wu, Y. B. Chen, J. M. Zhu, R. W. Peng, M. Wang, *Phys. Rev. B* **2016**, *93*, 054405.

[24] Y. Y. Weng, B. Zhang, S. J. Fu, M. Wang, R. W. Peng, G. B. Ma, D. J. Shu, N. B. Ming, *Phys. Rev. E* **2010**, *81*, 051607.

[25] Y. Wang, Y. Cao, M. Wang, S. Zhong, M. Z. Zhang, Y. Feng, R. W. Peng, X. P. Hao, N. B. Ming, *Phys. Rev. E* **2004**, *69*, 021607.

[26] S. Zhong, Y. Wang, M. Wang, M. Z. Zhang, X. B. Yin, R. W. Peng, N. B. Ming, *Phys. Rev. E* **2003**, *67*, 061601.

[27] M. Z. Zhang, Y. Wang, G. W. Yu, M. Wang, R. W. Peng, N. B. Ming, *J. Phys.: Condens. Matter* **2004**, *16*, 695.

[28] F. Chen, F. Yu, J. Li, R. W. Peng, M. Wang, unpublished.

[29] T. Dvir, B. Timko, D. Kohane, R. Langer, *Nat. Nanotechnol.* **2011**, *6*, 13.

[30] R. Huang, J. Heath, *Small* **2012**, *8*, 3417.

[31] S. Deng, V. Tjoa, H. M. Fan, H. R. Tan, D. C. Sayle, M. Olivo, S. Mhaisalkar, J. Wei, C. H. Sow, *J. Am. Chem. Soc.* **2012**, *134*, 4905.